Journal of the Korean Society of Remote Sensing, Vol. 10, No. 2, 1994

A Study on Comparison of Satellite-Tracked Drifter Temperature with Satellite-Derived Sea Surface Temperature of NOAA/NESDIS

Kyung-Ae Park* · Jong-Yul Chung* · Kuh Kim* · Byung-Ho Choi**

* Depertment of Oceanography, Seoul National Univ.

** Department of Civil Engineering, Sung Kyun Kwan Univ.

Abstract

Sea surface temperatures (SSTs) estimated by using the operational SST derivation equations of NOAA/NESDIS were compared with satellite-tracked drifter temperatures. As a result of eliminating cloud-filled or contaminated pixels through several cloud tests, 69 matchup points between the drifter temperatures and the SSTs estimated with NOAA satellite 9, 10, 11 and 12 data from August, 1993 to July, 1994 were collected. Multi-channel sea surface temperature (MCSST) using a split window technique showed an approximately 1.0℃ rms error as compared with the drifting buoy temperatures for 69 coincidences. Accuracies for satellite-derived sea surface temperatures were evaluated for only NOAA-11 AVHRR data which had relatively large matchups of 35 points as compared with other satellites. For the comparison of the observed temperatures with the calculated SSTs, linear MCSST and nonlinear cross product sea surface temperature (CPSST) algorithms by the split, the dual and the triple window technique were used respectively. As a result, the split window CPSSTs showed the smallest rms error of 0.72℃. Differences between the split window SSTs and the drifter temperatures appeared to have a linear tendency against the drifter temperatures and also against the differences between AVHRR channel 4 and 5 brightness temperatures. This indicates some possibilities that satellite-derived SSTs operationally calculated from the NOAA/NESDIS equations in the seas around Korea have been underestimated as compared with actual SSTs in case sea water temperature is relatively low or the atmosphere over the sea surface is very dry like in winter, while overestimated in case of high temperature or very moist atmospheric condition like in summer. So it is suggested that regional optimized SST retrieval equations based on local sea measurements around Korea instead of global measurements should be derived.

This study was supported in part by the Science Promotion Foundation and Basic Science Research Institute Program, Ministry of Education in 1993.

Introduction

During past several decades, numerous attempts have been made to derive sea surface temperatures from satellite data. Many SST retrieval algorithms have been developed by comparison of satellite data such as infrared data from Advanced Very High Resolution Radiometer (AVHRR) with shipboard measurements, buoy data or satellite-tracked drifting buoy data. Among those retrieval algorithms, a multi-channel sea surface temperature (MCSST) algorithm has been commonly utilized (e.g., Prabakahara, 1971 ; McClain, 1985). This familiar MCSST algorithm basically assumes a constant atmospheric absorption coefficient in estimating SST. Recently Walton(1988) developed the cross product sea surface temperature (CPSST) retrieval algorithm in which the atmospheric absorption parameters were dependent on the brightness temperatures of AVHRR. NESDIS (National Environmental Satellite Data and Information Service) of NOAA (National Oceanic and Atmospheric Administration) has been operationally produced SSTs using both the MCSST and the CPSST algorithm. SNU/RIO (Research Institute of Oceanography at Seoul National University) has applied the SST estimation equations published by NESDIS to the calculation of SSTs in the seas around Korea since November, 1989. But until now, there have been difficulties for these SSTs to be compared with in situ measurements because there were only a few coincident points between in situ observations and the satellite data, which should be sampled precisely at the same time and place as a satellite passes over. From this point of view, satellite drifting buoys can play an important role in lessening the difficulties on matching between the satellite data and the sea truth data. Two satellite-tracked drifters (20747, 20748) were deployed in the East Sea on August, 1993. Using these drifter data, accuracies of SSTs evaluated from the SST retrieval equations of NESDIS by the split, the dual and the triple window technique will be examined in this paper.

Data and Method

Two satellite-tracked drifter buoys (20747, 20748) were deployed in the northern part of the East Sea on August, 1993. The drifter 20747 has consistently given us a good quality temperatures and earth locations even till the present day(November, 1994). However, unfortunately the drifter 20748 lived just only for a few months because of a unknown cause. The temperature sensors of the drifters were located at a depth of approximately

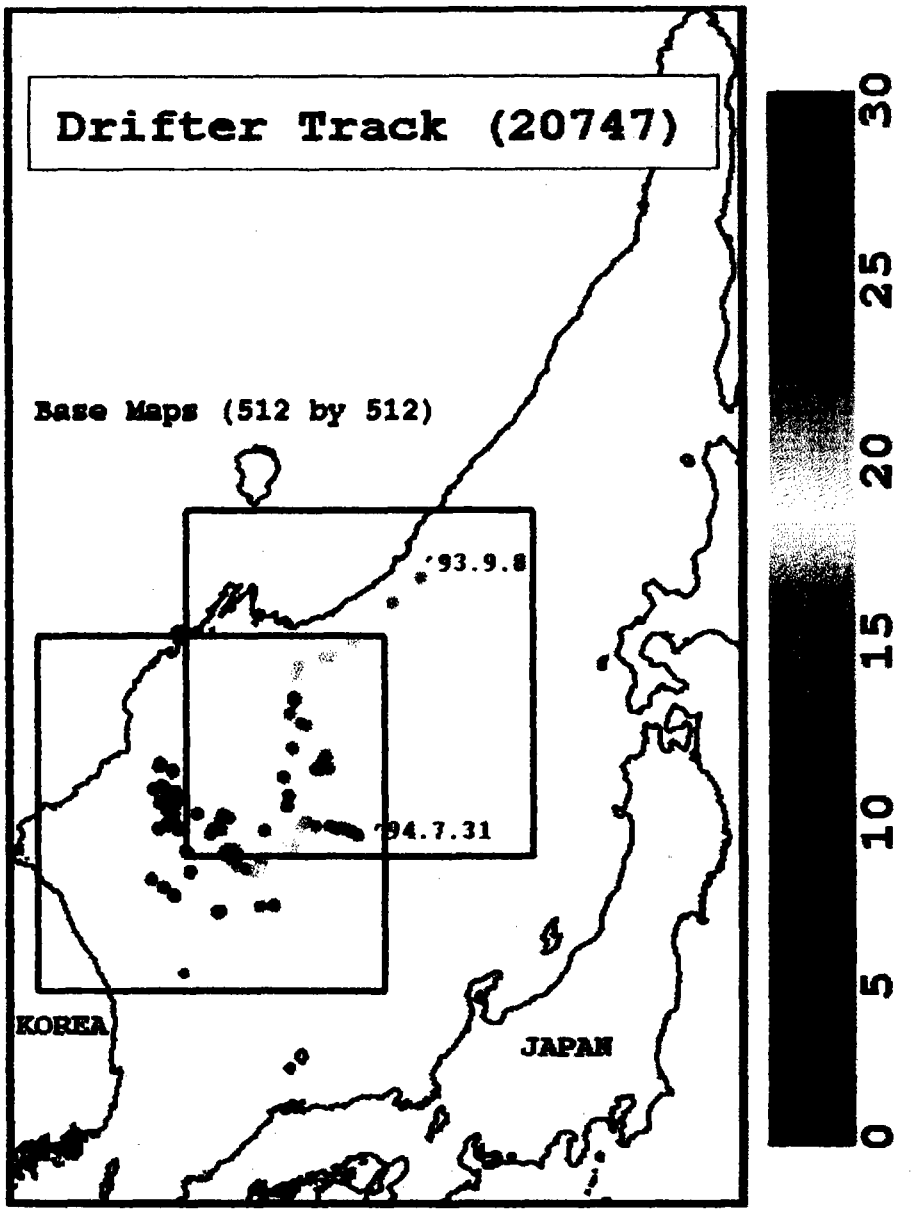

Figure 1. Track of the drifting buoy 20747 from August, 1993 to July, 1994. The two boxes represent basemaps for the extraction of AVHRR data. Color points represent the drifter temperature of the coincident earth locations.

20 centimeters below the water surface. Consequently the temperature measured by the drifters can be said to represent not a skin temperature but a subsurface temperature. Both the temperature data of the drifter 20747 and the 20748 from August, 1993 to July, 1994 were used in comparison of satellite SSTs. A series of matching procedures between the drifter data and the NOAA satellite data were done as following steps.

(a) A ground location of the drifting buoy was compared with the corresponding location on a ready-made AVHRR infrared image through routine works at SNU/RIO. At first, after scrutinizing by naked eyes whether the coincident locations were contaminated by cloud, only the pixels identified as non-contaminated were allowed to go to next steps.

(b) AVHRR data were extracted from HRPT on the basis of two base maps. For accurate geolocations of pixels, those maps were broadly composed of 512 by 512 pixel windows so as to include landmarks such as coastal lines or outlines of islands around the drifter location (Figure 1). These landmarks were useful for a geometric correction of an SST image.

(c) Extracted AVHRR channel 3, 4 and 5 data were radiometrically calibrated and converted into brightness temperatures using the procedure described by Lauritson et al.(1979). And also AVHRR channel 1 and 2 data were converted into albedo which would be used in cloud detection processes later.

(d) The images extracted against the basemaps were geometrically corrected through navigation procedures in which the geolocations theoretically calculated from satellite ephemeris were compared with the overlaid coastal lines and were navigated to the landmarks.

(e) The reference data such as the brightness temperatures or the albedo data of each channels and the satellite zenith angle for the matchup point between a drifter buoy location and a satellite image were extracted.

(f) The cloud-filled or contaminated pixels were detected and eliminated mainly by the detection technique by Saunders and Kriebel (1988). Pixels determined as clouds through a series of cloud detection algorithms were excluded at next processes. More details about the cloud detection algorithms will be described in the following section.

(g) The sea surface temperatures for the coincident points were derived from six different equations of NESDIS using the brightness temperature data set and the satellite zenith angles. And finally, the calculated SSTs were compared with the drifter temperatures.

Detailed procedures about the cloud detection and the removal of pixels with poor scanning geometry of a satellite sensor are described in the following sections.

1. Cloud Detection Methodology

Cloud detection algorithms are generally different for daytime and nighttime satellite data. Daytime cloud detection is relatively easier than nighttime because the visible reflectance of AVHRR data can be a very good discriminator of cloud contaminated pixels. In this study, only the data from 20 GMT to 01 GMT had been obtained because of an assigned operative duration of the buoy during a day. This interval corresponded to a morning time before or just after a sunrise in accordance with the seasonal variation of the sunrise time, so that the daytime algorithm of the cloud detection was alternatively used according to the availability of the visible reflectances of AVHRR channel 2 because of its distinguished properties about the cloud detection as compared with the nighttime algorithm. When the visible reflectance of each pixels were available, the albedo data of AVHRR channel 2 were used to detect the cloud contaminated pixels for the gross cloud and the spatial coherence test. If not available, the above tests were accomplished with the channel 4 brightness temperatures. The pixels exceeding 3% albedo or below -3℃ of the channel 4 brightness temperatures were regarded as cloud pixels and were excluded. A cloud free ocean showed quite a uniformly reflective characteristics as compared with a cloud-filled area, a cloud-contaminated area or a land. Using the reflective characteristics of the ocean surface, the spatial uniformity about the sea area was examined with the differences between a maximum and a minimum of the albedo data or the temperature data within 3 by 3 pixel window. The pixels exceeding each threshold were classified again as cloud contaminated pixels. Sea, cloud and land pixels appeared to have clearly discriminated peaks in the diagram with ch1/ch2 ratio. So the cloud contaminated pixels were also removed with these ratios, whose thresholds were used as same as Saunders and Kriebel(1988). Thermal fronts which had large temperature gradient were broadly distributed in the present study area, so that the higher threshold of the maximum-minimum difference within 3 by 3 window was selected so as not to exclude the oceanic thermal front area. Multi-spectral differences between each two channels were additionally used to detect misidentified pixels or various and complicated clouds such as a low cloud or a fog, a medium level cloud and a thin cirrus. Thresholds for each procedures were empirically determined. And more details about this discrimination procedures of cloud-filled or contaminated pixels are in progress for another publication.

2. Removal of Pixel with Poor Angle Geometry

Bernstein(1982) and Simpson(1990) used the four angles of a satellite cross track geometry such as the satellite zenith angle, the solar zenith angle, the solar reflection angle and the scattering phase angle in the conclusion of eliminating a poor quality data. In this study, two angle constraints of the satellite zenith angle and the solar reflection angle were selected to eliminate pixels with the poor angle geometry. First, pixels close to satellite swath edges were removed because the large satellite zenith angle at swath edges could make a longer atmospheric path than at a satellite nadir and give large errors in the calculation of SSTs. So pixels with the large satellite zenith angle over 53o were eliminated on the basis of the results of Bernstein (1982). Similarly solar radiation reflected on a sea surface gives rise to a sun glint on a satellite image in a certain condition. So the pixels lying too close to the sun glint were also excluded by considering the solar reflection angle which corresponded to the angle among a satellite, a satellite view point on the sea surface (nadir) and a reflected ray of sunlight. For the poor data removal, the limited cone angles of 20o - 30o around the expected line of specular reflection removal were selected as mentioned by Cox and Munk (1954), and this has been empirically verified at SNU/RIO. Only the pixels passing through these angle constraints related with the satellite scan track geometry were used for following comparisons.

3. Drifting Buoy Data

The Buoy 20747 was deployed at 43 14.98° N, 136 16.68° E at 16h 41min GMT on August 17, 1993 and the buoy 20748 at 42 8.33° N, 132 24.62° E at 9 hour 2 min GMT on August 24, 1993 offshore near Vladivostok in the northern part of the East Sea. Sea surface temperatures were measured by a temperature sensor inside the buoy at a depth of about 20 cm below the sea surface. The temperatures measured by the drifter buoy sensor were sampled and broadcast to the DCLS (Data Collection and Location System) on the NOAA series of polar orbiting weather satellites. Judging from a dynamical viewpoint about the processes on the sea surface, the present drifter data were regarded as nighttime data rather than daytime data because they were collected from 4 to 9 o'clock in Korean standard time, when the vertical stratification of temperatures near the sea surface had not yet strongly established due to a small solar insolation and an insufficient heating during this duration except a critical situation of summer. With these reasons, both the drifting buoy data and the satellite data were regarded as nighttime data and compared with SSTs from nighttime SST retrieval equations

4. Sea Surface Temperature Estimation

A general form for multi-channel sea surface temperature retrieval algorithms using AVHRR brightness temperatures is:

$$MCSST = T_i + A\,(T_i - T_j) + B \tag{1}$$

where T_i and T_j are brightness temperatures at two different wavelengths, the coefficients A and B represent an atmospheric absorption coefficient and a regression constant respectively. Two or three pairs of spectral windows have generally been used in the derivation of SST. The split window technique uses AVHRR channel 4 and 5 brightness temperature, and the dual window uses AVHRR channel 3 and 4 brightness temperatures as in the above formulas. The triple window technique is based on three infrared channels of AVHRR for the SST retrieval as following:

$$MCSST = AT_j + B\,(T_i - T_k) + C \tag{2}$$

where T_i, T_j, T_k corresponds to the satellite measured brightness temperature of AVHRR channel 3, 4 and 5 respectively and A, B, C are the regression coefficients. In more recent studies, the coefficients in equation (2) were reported to have some dependencies on the air mass of the atmosphere. The attenuation of infrared radiances due to this long atmospheric path length has been removed somewhat by considering satellite viewing angle in the estimation of the sea surface temperatures. So a new technique considering the satellite zenith angle for an scanning pixel was developed and has been widely used until now as following form:

$$MCSST = AT_i + B(T_i - T_j) + C(T_i - T_j) * (\sec sza - 1) + D(\sec sza - 1) + E \tag{3}$$

where $\sec sza$ means secant of the satellite zenith angle. NOAA/NESDIS has produced SSTs operationally according to the above formula. Table 2 shows the split window multi-channel sea surface temperature estimation equations for each NOAA satellite for the daytime and the nighttime data.

Table 1. Distributions of matchup points between drifter data and AVHRR data.

Sat. ID	NOAA-9		NOAA-10		NOAA-11		NOAA-12		
Drifter ID	20747	20748	20747	20748	20747	20748	20747	20748	Total
'93 Aug.									
Sep.				1	4		4		9
Oct.			2		5		1	2	10
Nov.		3	2	1	3		1	3	13
Dec.					1		1		2
'94 Jan.					1				1
Feb.					1				1
March	1								1
April					4				4
May	1				5		1		7
June			3		6		1		10
July	2		3		5		1		11
Total	4	3	10	2	35		10	5	69

More recently, Walton(1988) developed a non-linear sea surface temperature estimation algorithm, CPSST(cross product sea surface temperature) method. He suggested that the CPSST algorithm can lessen SST errors for dataset containing random noises such as AVHRR channel 3 data. The fundamental form including the satellite zenith angle effects of CPSST is as follows :

$$CPSST(i,j) = \frac{T_i SST_j - T_j SST_i}{T_i - T_j + SST_j - SST_i} \tag{4}$$

$$\begin{aligned} SST_i &= A_i T_i + B_i \\ SST_j &= A_j T_j + B_j \end{aligned} \tag{5}$$

T_i, T_j : brightness temperature at two different wavelengths i and j

A_i, B_i : regression coefficients of AVHRR channel i

A_j, B_j : regression coefficients of AVHRR channel j

where SST_i and SST_j are the sea surface temperatures estimated by a single channel regression method. Table 3 shows MCSST and CPSST equations for only NOAA-11. They were classified on the basis of three window techniques as mentioned above. The sea surface temperatures calculated by these two algorithms were compared with the satellite drifting buoy data.

Results

As a result of eliminating pixels contaminated with clouds and with the poor satellite scan track geometry, 69 pairs of coincident points between satellite data and the drifter buoy locations were collected from all the available NOAA satellite data from August, 1993 to July, 1994. They were composed of 35 points from NOAA-11 data, 15 from NOAA-12, 12 from NOAA-10 and 7 points from NOAA-9 respectively as described at Table 1. Coincident points from NOAA-11 were much more numerous than those from other NOAA satellites. There were a few points from the drifter 20748 because of its short operative duration. Monthly distributions of the matchup points at Table 1 show that there were quite a few coincidences in winter from December, 1993 to February, 1994.

Table 2. Split window MCSST estimation equations for NOAA/AVHRR data by NOAA/NESDIS. sza means satellite zenith angle, and D and N represent daytime and nighttime respectively.

MCSST = A*T4 + B*(T4-T5) + C*(T4-T5)*(SEC(sza)-1) + D*(SEC(sza)-1) + E

Sat. ID	Time	A	B	C	D	E(K)	E(C)
NOAA-12	D	1.013674	2.443474	0.314312	0.0	-4.647	-0.912
	N	1.013674	2.443474	0.314312	0.0	-4.647	-0.912
NOAA-11	D	1.01345	2.659762	0.526548	0.0	-4.592	-0.918
	N	1.052	2.397089	0.959766	0.0	-15.52	-1.316
NOAA-9	D	0.9994	2.7057	-0.27	0.73	0.1177	-0.046
	N	0.9994	2.7057	-0.27	0.73	0.1177	-0.046
NOAA-10	D	1.1	0.0	0.0	0.0	-27.316	0.0
	N	1.1	0.0	0.0	0.0	-27.316	0.0

This resulted from the difficulties in getting the cloud free matchup points because the East Sea had been occasionally masked with cloud which might result from the prevailing northwest winds around Korea in winter. In order to estimate accuracies of satellite SSTs retrieved by NESDIS equations in the East Sea, all the available AVHRR data of each NOAA satellites were used. Table 2 shows several SST estimation equations used by NOAA/NESDIS(1991). The split window equations using both

AVHRR channel 4 and channel 5 brightness temperatures include the satellite viewing angle correction terms to reduce the estimation error from the sensor scanning angle. D and N in Table 2 indicate the daytime and the nighttime coefficients respectively, and the satellite zenith angle was represented as sza. It is seen other satellites except NOAA-11 use the same coefficients irrespective of time of the day, while NOAA-11 has different ones according to the daytime or the nighttime pass. And it should be noted that SSTs using NOAA-10 AVHRR data were calculated by just multiplying 1.1 to the channel 4 brightness temperature because AVHRR radiometer of NOAA-10 did not include channel 5 wavelengths. First of all the comparisons were made with only the split window equations because the dual and the triple window equations requiring AVHRR channel 3 brightness temperatures can generate a large SST error due to the electronic noises of channel 3 itself. Figure 2 shows the comparison of the drifter temperatures and the satellite SSTs for 69 coincident points. The range of the drifting buoy temperatures varied from 4℃ to 27℃. Although critical temperature data near 0℃ or high temperatures over 27℃ were insufficiently collected, the present data set may be regarded as representing the typical distribution of the sea surface temperatures in the East Sea. The straight line in Figure 2 represents a perfect agreement line between the buoy temperatures and the calculated SSTs. There was a general consistency between the two temperatures with approximately 1.0℃ rms (root mean square) error. Most of calculated MCSSTs appeared to have some deviations within ±2℃ against the observational drifter temperatures except a few points.

The number of matchup points of NOAA-9, 10, 12 except NOAA-11 was too small for the satellite-derived SSTs to be compared with the sea truth measurements. So the comparison was made for only NOAA-11 data which had relatively large coincident points. Nighttime MCSST and CPSST equations with NOAA-11 AVHRR data for the three window techniques are shown in Table 3. 35 point data were extracted and used to calculate SSTs by those equations. The dates at Table 3 indicate the revised date of those equations by NOAA/NESDIS. Three kinds of the MCSST equations revised on September 27, 1989 by NOAA/NESDIS have been used in the calculation of SSTs at SNU/RIO.

Walton(1988) mentioned that the CPSST technique as a nonlinear algorithm could reduce random or noncorrelative error in estimating SSTs. The CPSST equations revised on April 18, 1990 have not been operationally used at SNU/RIO, but they were chosen here for the comparison and for the applicability to the Korean waters.

Table 3. MCSST and CPSST estimation equations for NOAA-11 by NOAA/NESDIS(1991). Units are ℃ in ℃ out for MCSST and ℃ in °F out for CPSST. Date represents the revised date for each equation and a satellite zenith angle is represented as sza.

Method	Window	Equations	Date
MCSST	split	1.052*T4 + 2.397089*(T4-T5) + 0.959766*(T4-T5) *(SEC(sza)-1) - 1.316	'89.9.27
	dual	1.03432*T4 + 1.347423*(T3-T4) + 0.953042*(T3-T4) *(SEC(sza)-1) + 1.730466	'89.9.27
	triple	1.036027*T4 + 0.892857*(T3-T5) + 0.520056*(T3-T5) *(SEC(sza)-1) + 0.61680805	'89.9.27
CPSST	split	$\frac{0.19596*T5 - 48.61}{0.20524*T5 - 0.17334*T4 - 6.11}(T4 - T5 + 1.46)$ + 0.95476*T5 + 0.98*(T4-T5)*(SEC(sza)-1) - 263.84	'90.4.18
	dual	$\frac{0.17079*T4 - 58.47}{0.17334*T4 - 0.07747*T3 - 33.74}(T3 - T4 - 6.44)$ + 0.98530*T4 + 1.97*(SEC(sza)-1) - 257.28	'90.4.18
	triple	$\frac{0.16835*T5 - 34.32}{0.20524*T5 - 0.07747*T4 - 20.01}(T3 - T5 + 14.86)$ + 0.97120*T5 + 1.87*(SEC(sza)-1) - 276.59	'90.4.18

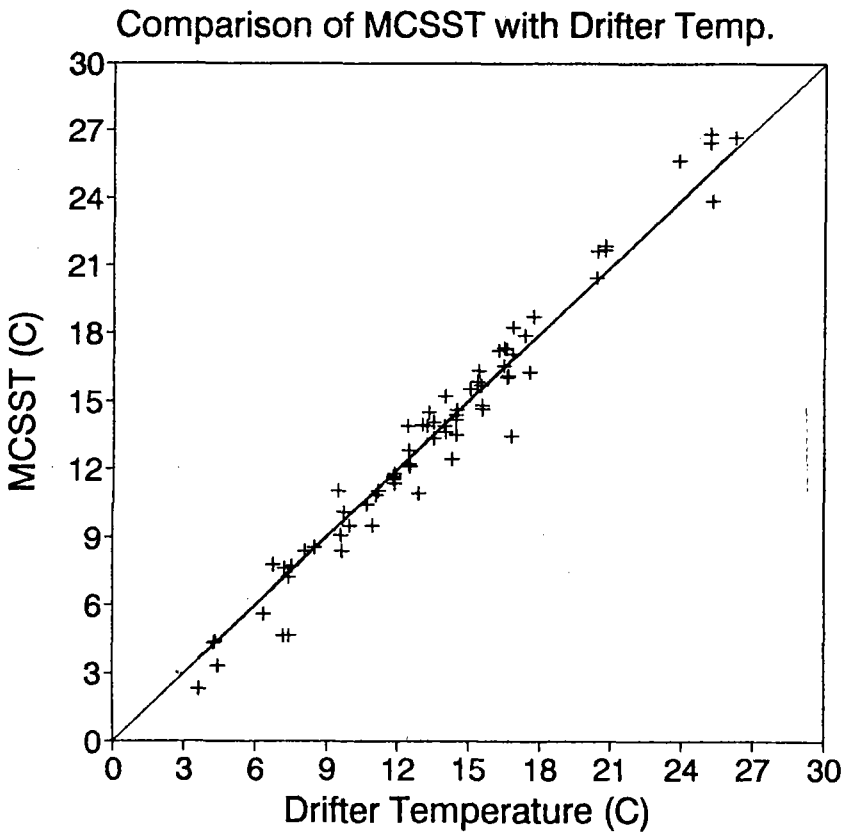

Figure 2. Comparison of drifter temperatures with sea surface temperatures by the operational split window equations of NOAA/NESDIS for 69 coincident points.

Bias and rms errors for SSTs estimated with the above six equations were presented at Table 4. The correlation values represent normalized correlation coefficients between the satellite calculated SSTs and the drifter temperatures as actual observations. The split window CPSST technique showed the smallest rms error of 0.72℃ out of six equations, and in addition the MCSST technique using the same window showed the secondly smallest rms error of 0.91℃ at Table 4. CPSSTs estimated by the dual or the triple window equations had large rms error over 1℃. From the fact that the rms errors for both the split window MCSSTs and CPSSTs

Table 4. SST estimation errors and correlation coefficients for MCSST and CPSST equations.

Method	Window	bias	rms	Correlation
MCSST	Dual	-10.84341	1.36922	0.9743
	Split	15.99489	0.91157	0.9959
	Triple	-1.59791	0.91079	0.9871
CPSST	Dual	-16.66561	1.52882	0.9635
	Split	11.61729	0.72939	0.9978
	Triple	-43.00401	1.65100	0.9839

appeared to be smaller than other window, the split window technique can be assumed to be the best tool in estimating SSTs using AVHRR data. This was also verified with the correlation coefficients between the observed and the calculated temperature. The coefficients for the MCSSTs and the CPSSTs using the split window showed large values of 0.9959 and 0.9978 respectively. Especially the split widow CPSST showed an improved and excellent consistency of approximately 0.9978 with actual observations. Judging from the present dataset, it seems that the split window CPSST technique is the best tool to estimate sea surface temperatures from the satellite infrared data. However, the large bias errors of all the six equations indicate the calculated SSTs were not balanced about the perfect agreement line with the drifter temperatures.

Figure 3 shows the comparison of drifter temperatures with MCSSTs for NOAA-11 AVHRR data by the dual, the split and the triple window technique. The points in the diagram represents the deviations of the calculated temperatures from the measured drifter temperatures (MCSST minus drifter temperature). Distinct features for each windows can be recognized in the distributions of temperature differences. In case of the dual window technique the differences were widely scattered as could be seen in (a) of Figure 3. Their ranges by the dual window amounted to roughly ±3℃ and those by the triple window varied within ±2℃. Especially the dual window SSTs were revealed to have large scatters of the temperature difference distribution at relatively low drifter temperature range near from 4℃ to 8℃ (Figure 3-(a)). Large temperature differences within this range were also found for the triple window SSTs as displayed in Figure 3-(c).

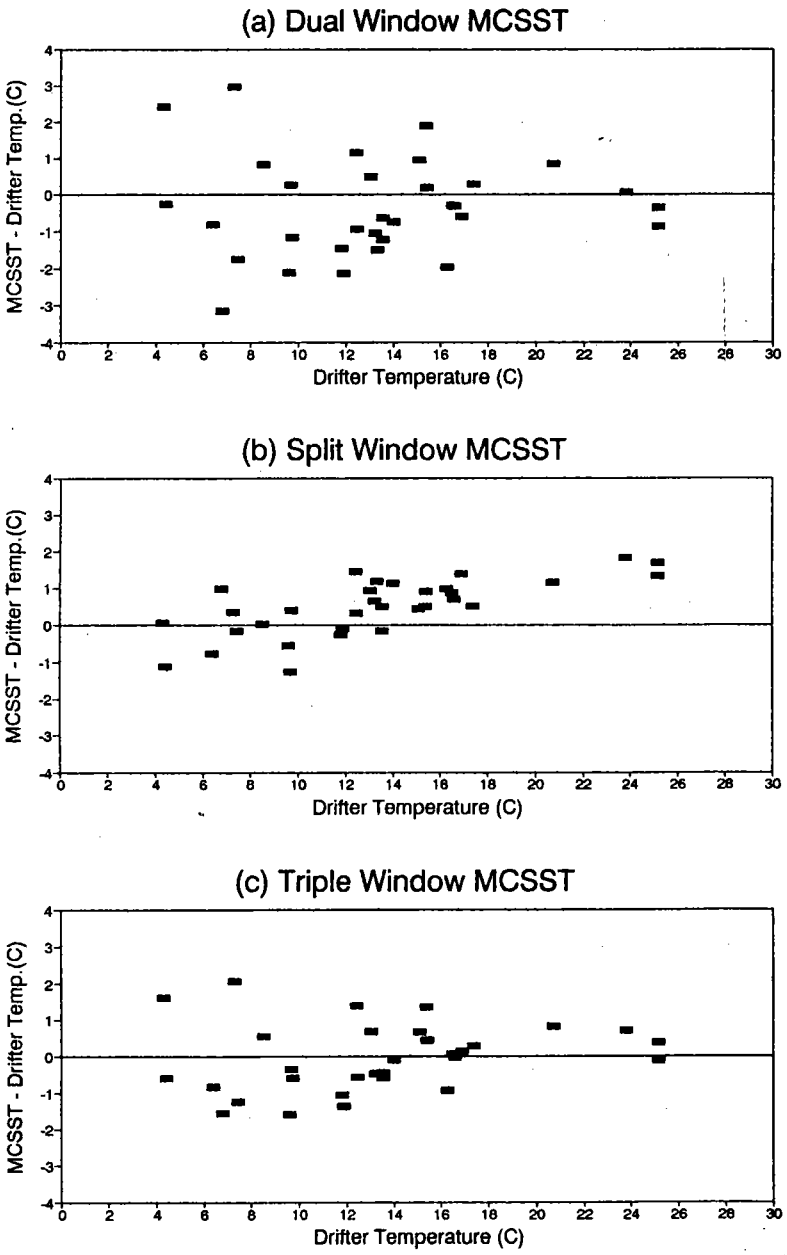

Figure 3. Comparison of MCSSTs for NOAA-11 data with drifter temperature. (a), (b) and (c) results from the dual window, the split window and the triple window technique respectively.

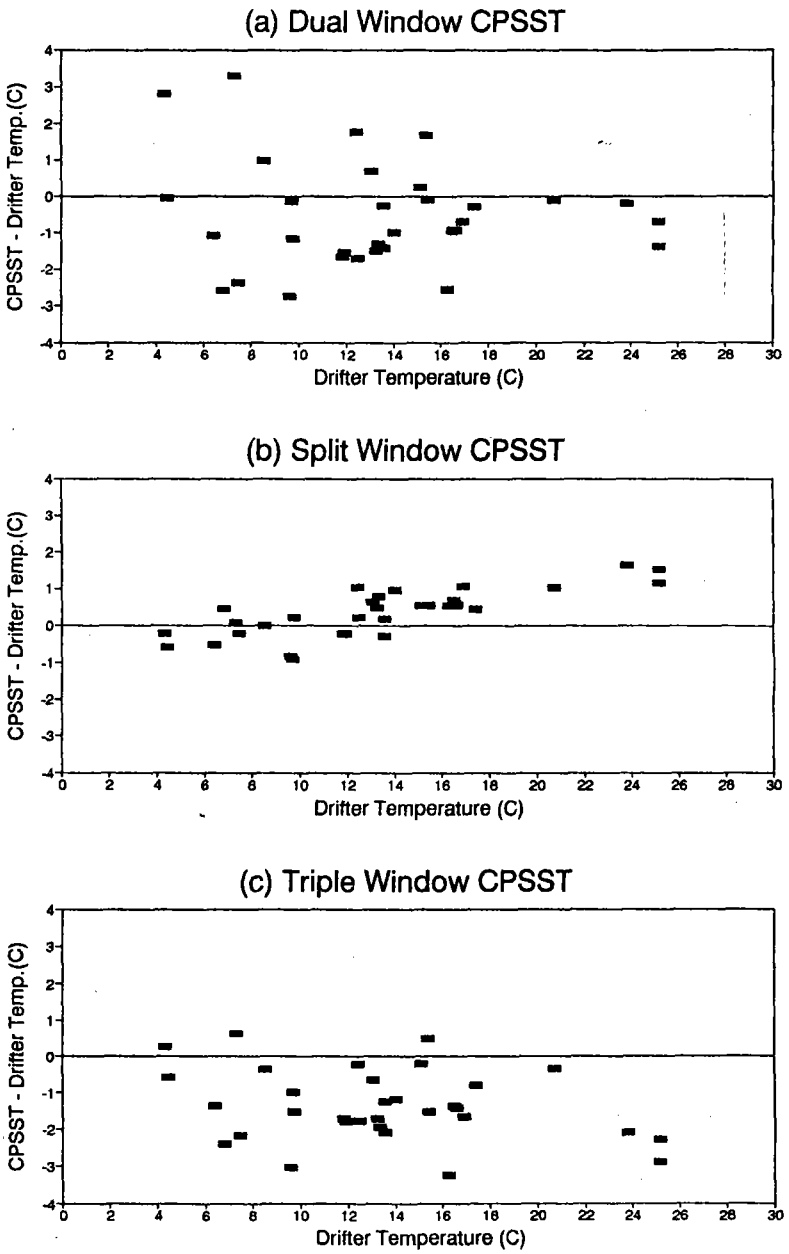

Figure 4. Comparison of CPSSTs for NOAA-11 data with drifter temperature. (a), (b) and (c) results from the dual window, the split window and the triple window technique respectively.

Based on the above results, when large contribution of solar radiation or the channel 3 noises were expected, SST estimation techniques excluding the AVHRR channel 3 data proved better. However the AVHRR channel 3 data can give better results for noise free data because they are less influenced by water vapor in the atmosphere than other wavelength of channel 4 or channel 5. However, these features didn't appear at the split window MCSSTs. The MCSST deviations from the drifter temperature had much less scatter. The fact, that the large scatter of differences didn't appear at split window (Figure 3-(b)) and the general pattern of temperature deviations of the dual and the triple window SSTs had a similarity in the shape of their distributions, indicates these deviations of the dual and the triple widow SSTs may be inferred from the noises of AVHRR channel 3 brightness temperatures. The large deviations of the dual or the triple window SSTs were also found at the result of CPSSTs as displayed in Figure 4-(a) and (c). The triple window CPSSTs appeared to underestimate actual SSTs (Figure 4-(c)). And both the MCSSTs and the CPSSTs estimated by the dual or the triple window showed large scatter distributions of comparison points. On the other hand, both of split window MCSSTs and CPSSTs show much smaller rms error of 0.9℃ and 0.72℃ than other method (Figure 3-(b), Figure 4-(b)). However, some tendencies were detected in the results of the split window SSTs. Temperature deviations of the satellite-retrieved SSTs from the drifter temperatures were positive when the drifter buoy temperatures were high above 20℃, while, negative for low temperatures below 10℃. This means that the satellite-retrieved SSTs were estimated higher than sea truth measurements in the range of high temperature and evaluated lower in the low temperature range (Figure3-(b)). And also, these were distinctly found for the CPSSTs by the split window technique as shown in Figure 4-(b). Similarly to the MCSST case, the differences by the split window CPSST calculation gradually changed from negative to positive as the drifter temperatures increased. It seemed that the tendency of CPSSTs had much stronger linearity than that of MCSSTs owing to the small scatter of the temperature difference for sea truth observations. These tendencies may be guessed to be related with some variations of atmospheric conditions over the seas around Korea such as in summer or winter at a mid-latitude region. So, the atmospheric conditions in present dataset were indirectly guessed by examining differences between AVHRR channel 4 and channel 5 brightness temperatures. Figure 5 shows the distributions of the temperature differences between AVHRR channel 4 and channel 5 brightness temperatures (T4-T5) versus the drifter temperatures. It was reported that for cloud free pixels a dry and cold atmosphere generally have differences less than 1℃, while a warm

and moist atmosphere shows high values over 1℃ (Saunders and Kreibel, 1988). In the present data set, the differences amounting to 2.5℃ were regarded to correspond to summertime data and the smaller differences of approximately 0.2℃ were regarded as wintertime data.

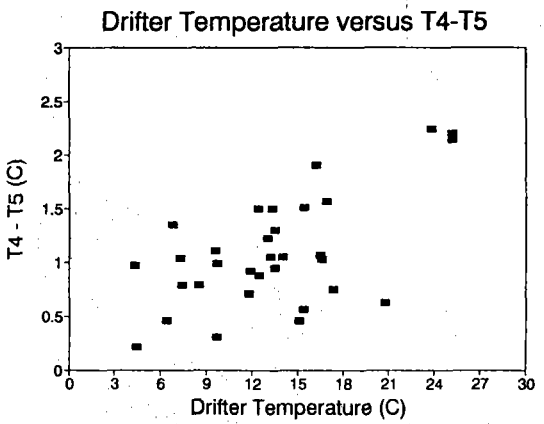

Figure 5. Variations of differences between AVHRR channel 4 and channel 5 brightness temperature versus the drifter temperature.

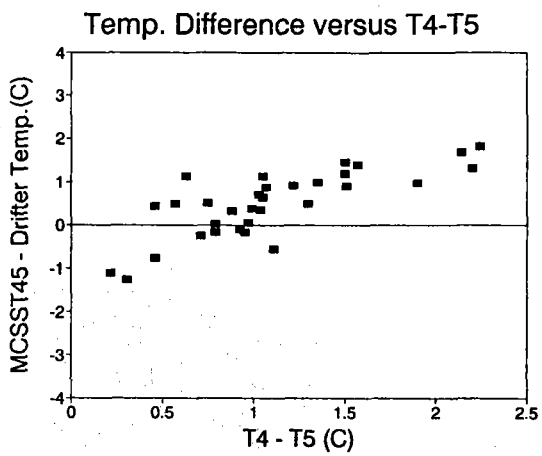

Figure 6. Variations of differences between the calculated split window MCSST and the drifter temperature versus differences between AVHRR channel 4 and channel 5 brightness temperature.

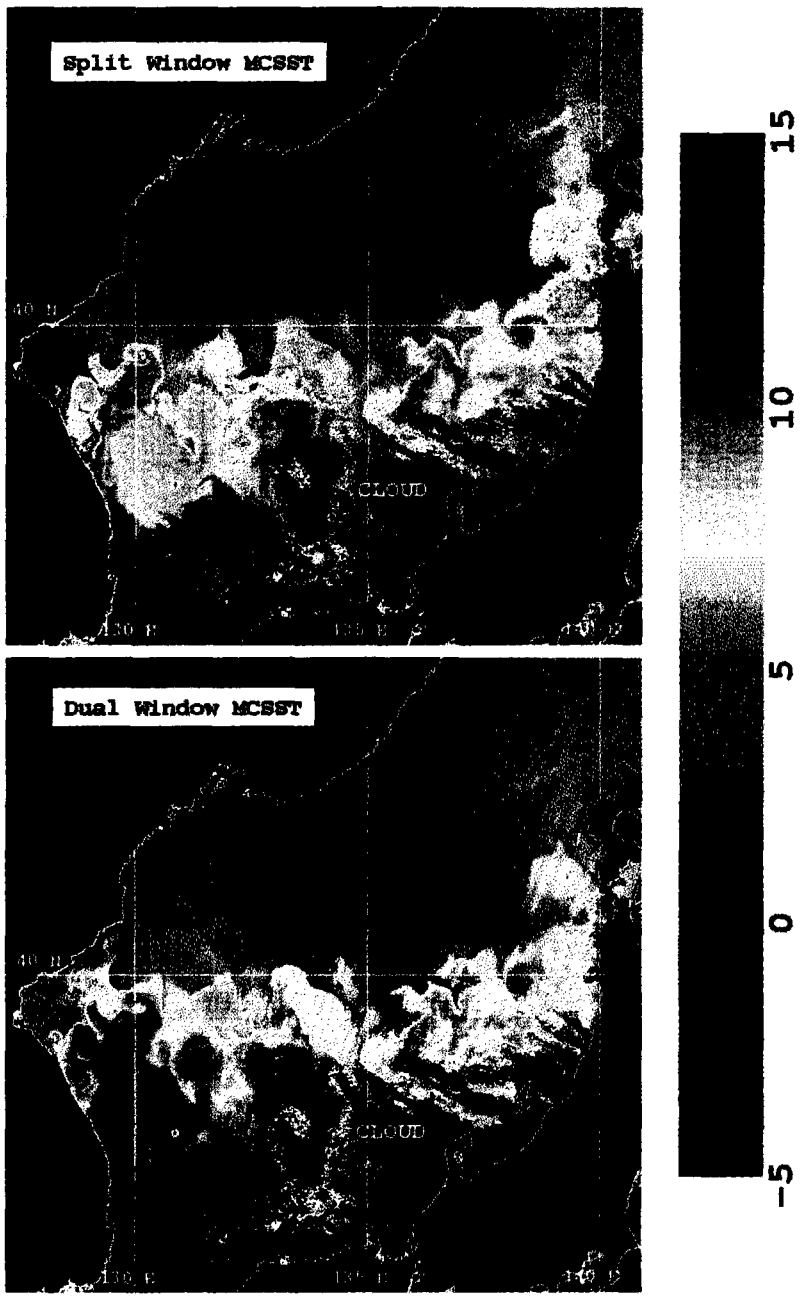

Figure 7. Horizontal distributions of multi-channel sea surface temperature estimated by the dual window and the split window equation in the East Sea in early March, 1990.

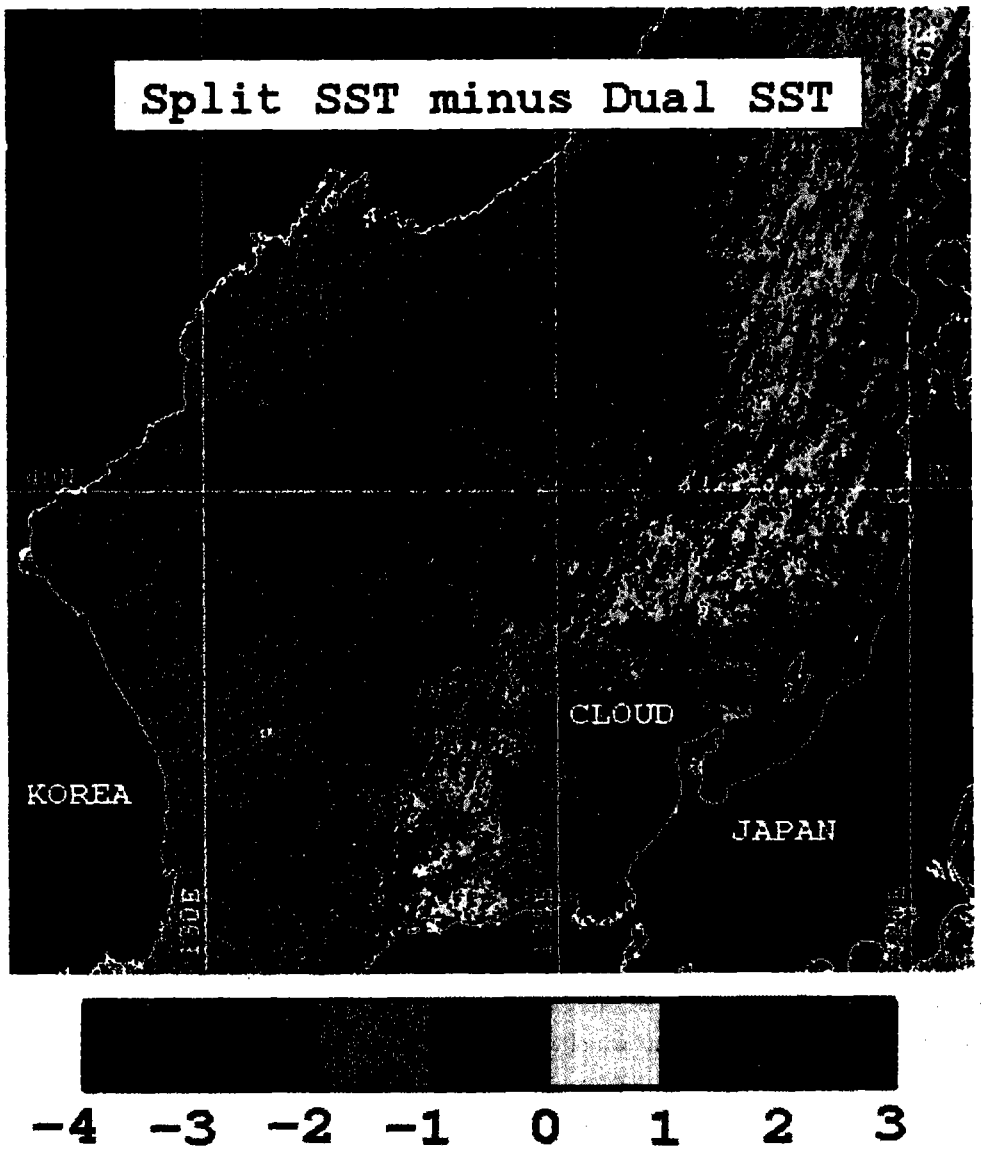

Figure 8. Horizontal distributions of the split window SST minus the dual window SST using the same AVHRR data.

Accordingly the atmosphere above the sea surface in the East Sea were supposed to be under a dry and cold condition in winter and a moist and warm condition in summer. Under these different atmospheric conditions, the differences between the split window MCSSTs and the drifter temperatures were examined in Figure 6. The linear tendency was also appeared markedly, so that satellite SST errors about sea truths had an strong dependence upon the atmospheric conditions over the sea surface. Consequently the satellite-derived SSTs using the split window showed better consistency than any other window, but there were some tendencies to underestimate or overestimate SSTs as compared with sea truth measurements under a certain critical atmospheric condition such as a very moist or a most dry atmosphere over the seas around Korea. These have been detected actually in SST images by the split window estimation for the same satellite pass at SNU/RIO.

Figure 7 represents the distributions of the split and the dual window MCSSTs for the same nighttime satellite in early March, 1990. Typical cloud distributions over the East Sea in January or February every year prevent from getting clear SSTs. So as an example, in order to examine the underestimation phenomenon of SSTs in winter in two dimensional horizontal SST distribution, the early March image whose atmosphere is under a condition similar to that of winter was selected. And for the distinct discrimination of cold and warm SSTs, the rainbow colors from -5℃ to 15℃ were rendered on the image. Blue colors represent low temperature and red colors in southern part show relatively high sea surface temperature. The features like the diagonal and the regular straight line on the dual window SST image may be considered as noises caused by inclusion of AVHRR channel 3 instrumental noises in the calculation of SSTs. The horizontal SSTs showed large differences over 10℃ between northern and southern part of the East Sea. Comparing the MCSSTs by the two windows, it was easily seen the split window SSTs were much lower than those of the dual window in the overall portions of the East Sea. Especially it should be noted the split window SSTs at offseas near Vladivostok appeared to be much colder than the dual window SSTs.

And a quantitative analysis about these two dimensional temperature differences was constructed at Figure 8. Figure 8 shows the horizontal distributions of temperature differences between the split window MCSSTs and the dual window MCSSTs for the same pixel. These varied from -4℃ to 3℃, but most of the pixels were negative values except for pixels on the right side in the image. The positive signs of pixels may be thought to result from their large swath angles. Actually the positives at Figure 8

correspond to the right edges of a sensor scanning on the earth surface with large satellite zenith angles. Kelly(1986) has suggested this satellite viewing angle or the satellite zenith angle may be a primary cause of temperature error. And Berstein(1982) pointed out that SSTs were reliable only through a removal of poor viewing geometry over 53° .

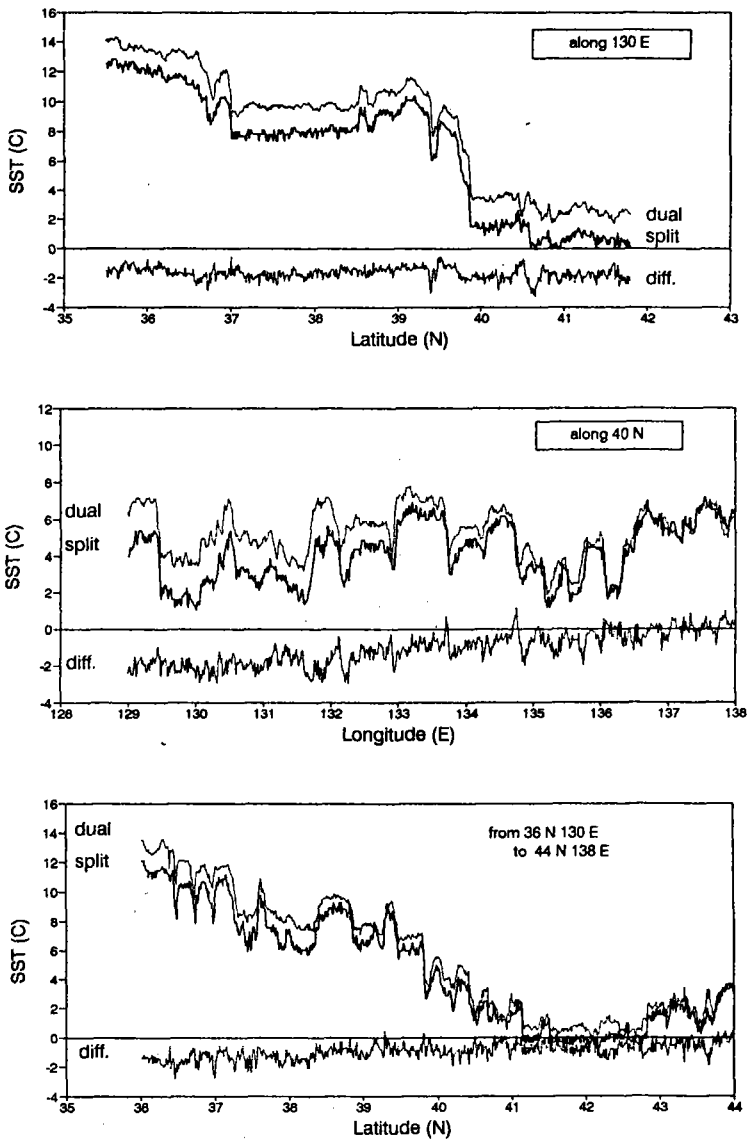

Figure 9. Variations of the split and the dual window SSTs and their differences(split minus dual) along 130° E, 40° N and along diagonal from 36° N, 130° E to 44° N, 138° E.

Hence, the temperatures of most pixels in Figure 8 could be assumed underestimated as compared with the sea truths in winter. This was better analyzed quantitatively through a latitudinal or a longitudinal cross section about the distribution of SSTs. Three profiles were made along longitudinal line of 130° E, along the latitudinal line of 40° N and along the diagonal from 36° N 130° E to 44° N 138° E about SSTs as displayed at Figure 9. The underestimation of the split window satellite SSTs as compared with the dual window satellite SSTs systematically appeared at all of three profiles. The upper and middle line at each diagram indicate SST variations of the dual and the split SSTs respectively. And the below third line corresponds to differences of the two SSTs (split minus dual). Most of the temperature differences along 130° N had negative values and also most of the pixels along 40° N and along the diagonal from 36° N, 130° E to 44° N, 138° E except for a few pixels lying at large swath edges showed negative values. Mean of the differences along these three cross section appeared to be -1.69, -1.08, -0.94 respectively as in the upper diagram in Figure 9. Differences of more or less than -1.0℃ were detected at SST images by the different window methods. Though the split window SSTs were compared with only the dual window SSTs instead of actual sea measurements, it can be said at least through this study that the split window SSTs can underestimate or overestimate under the critical atmospheric condition such as in summer or in winter. Potential dynamics to explain these results will be discussed at following section.

Concluding Remarks

In this paper an attempt has been made to compare satellite-estimated sea surface temperatures using NOAA/NESDIS equations with sea truth measurements in the East Sea. A detailed examination of NOAA satellite data and temperature observations by the drifting buoys produced a data set comprising 69 pairs in the northern part of the East Sea. In generating this data set, cloud filled or contaminated pixels with a small portion of cloud within a pixel size or a unresolved cloud were detected and eliminated with several removal steps suggested by Saunders and Kriebel (1988). The gross cloud test and the horizontal uniformity of a cloud field were made and albedo or AVHRR brightness temperature were checked for nighttime data. Brightness temperature differences between two spectral bands among three infrared channels of AVHRR were used to remove various type of clouds and pixels with poor satellite viewing angle were also eliminated.

Comparison of the drifter buoy temperature with AVHRR-based SSTs for 69 pairs showed an rms error of approximately 1.0℃. Considering this comparison was made only by the split window MCSST equations, poorer accuracies over 1℃ are expected if the dual or the triple window SSTs which include an instrumental noise of AVHRR channel 3 are used. Hence this means that the split window equations of NOAA/NESDIS producing operationally for four NOAA satellites at SNU/RIO can estimate sea surface temperature with an uncertainty level of approximately 1.0℃ in the sea around Korea.

Accuracies for various MCSST and CPSST equations were estimated for NOAA-11 AVHRR data because other satellites had only a few matchup points. 35 coincident pairs of NOAA-11 were made and used to evaluate an error of satellite SSTs. The split window SST retrieval technique used in calculating MCSSTs and CPSSTs was revealed as the best tool of all the windows with an small rms error of 0.72℃ and 0.91℃ respectively. However the SSTs by the dual or the triple window technique showed large scatters about the drifter temperatures, which may result from AVHRR channel 3 noises from the electronic interference of AVHRR sensor itself. In addition considering most of dataset in the present study corresponded to just before or just after sunrise, it is inferred a solar radiation at 3.7 μm in this dataset is larger than sea water itself (Robinson,1985). Accordingly if the large contribution of solar radiation like in some portions of this data set is expected, it indicates the SST estimation technique like the split window technique excluding AVHRR channel 3 data would be better. While, AVHRR channel 3 data give better results at noise free data because those are less contaminated by a water vapor in the atmosphere than other channel data.

It should be noted that there existed a linear relationship in differences between the satellite SSTs and the drifter temperatures by the split window technique as shown at Figure 3-(b) and Figure 4-(b). Differences (satellite SST minus the drifter temperature) by MCSST or CPSST technique showed a gradual increase from negative to positive as the drifter temperatures increased. This suggests that NESDIS operational equations should be partially corrected for the East Sea. For cloud free pixels, the dry and cold atmosphere was reported to have differences (channel 4 minus channel 5) less than 1℃, while warm and moist atmosphere has large values over 1℃(Saunders, 1986). So the atmospheric condition in present dataset was indirectly examined with differences between AVHRR channel 4 and channel 5 data. From Figure 5, the atmospheric condition above sea surface was assumed to be dry and cold condition in winter and moist in summer. It also appeared at Figure 6 that differences between the split window MCSST and the drifter temperature gradually

were increased as those between AVHRR channel 4 and 5 brightness temperature increased. In other words, the satellite SSTs operationally produced at SNU/RIO using NESDIS equations might have given much lower or much higher temperature than a real sea truth measurement under certain atmospheric conditions. If so, some cautions should be required to estimate sea surface temperatures from NOAA satellites in the seas around Korea. And also these phenomena were actually detected in the SST image made by the split window estimation as compared with dual window images for the same satellite data (Figure 7), and were quantitatively analyzed by getting temperature differences between the two windows (Figure 8). Most pixels showed negative values, that is, split window SSTs were lower than the dual window SSTs. And the cross sectional profiles for both SSTs also showed the systematic underestimation of the split window MCSSTs as in Figure 9.

It seems that these overestimation and underestimation of sea surface temperature are associated with the difference between a bulk temperature and a skin temperature of sea water. AVHRR infrared data correspond not to a bulk temperature but to the oceanic skin temperature. To observe the skin temperature under a real oceanic condition is almost impossible. For that reason, the subsurface temperatures have been measured by a buoy or a ship etc. and have been used in retrieving the regression equations of satellite SSTs instead of the skin temperature. Thus the infrared data measured at a surface film are thought to be forcibly adjusted to the bulk temperature through numerous regressions using similar algorithms until now. Atmosphere over the sea surface around Korea in winter appeared to have very dry and cold characteristics. When an air mass passes over the sea surface, heat is transferred from the sea surface to the atmosphere, so the temperature of sea surface becomes colder than the subsurface. On the contrary, in summer, the sea surface temperature becomes higher than the subsurface temperature owing to a strong solar insolation at the sea surface. These bring about large differences between the oceanic skin and the subsurface temperature. Hence it indicates that these can be one of possible explanations about the linear tendency in this study as mentioned above.

The linear tendency of temperature differences in applying NOAA/NESDIS equations to the evaluation of SSTs in the sea neighbouring Korea points out that a certain data set which has been used for SST regressions at NESDIS could insufficiently include the various oceanic and atmospheric conditions at a local scale. This suggests SST retrieval equations should be regionally optimized on the basis of local sea measurements instead of global measurements, and in addition some studies relating the ocean skin temperature and the bulk temperature is required.

References

Bernstein R.L., 1982, Sea surface temperature estimation using the NOAA-6 satellite Advanced Very High Resolution Radiometer. J. Geophy. Res., 87, C12 p9455-9465.

Cox C.S. and Munk W.H., 1954, Measurements of the roughness of the sea surface from photographs of the sun's glitter, J. Opt. Soc. Am., 44, p838-850.

Kelly K.A. and Davis R.E. 1986, An analysis of errors in sea surface temperature in a series of infrared images from NOAA-6. J. Geophy. Res., 91, C2, p2633-2644.

Lauritson et al., 1979, Data extraction and calibration of TIROS-N/NOAA radiometers. NOAA technical Memo NESS 107(Washington,D.C.:NOAA)

McClain E.P., Pichel W.G. and Walton C .C., 1985, Comparative performance of AVHRR-based multichannel sea surface temperature. J. Geophy. Res., 90, p3655-3661.

NOAA/NESDIS, 1991, NOAA Polar Orbiter Data Users Guide, compiled and ed. by K.B. Kidwell, NOAA/NESDIS

Prabakahara C., Dalu G. and Kunde V.G., 1974, Estimation of sea surface temperature from remote sensing in the 11 - 13 μm window region, J. Geophy. Res., 79, p5039-5044.

Robinson I.S., 1985, Satellite Oceanography, Ellis Horwood Limited, p455.

Saunders R.W., 1986, An automated scheme for the removal of cloud contamination from AVHRR radiances over western Europe, *Int. J. Remote Sensing*, 7, p867

Saunders R.W. and Kriebel K.T., 1988, An improved method for detecting clear sky and cloudy radiances from AVHRR data. *Int. J. Remote Sensing*, 9, p123-150.

Simpson J.J. and Humphery C., 1990, An automated cloud screening algorithm for daytime Advanced Very High Resolution Radiometer Imagery, J. Geophy. Res., 95, C8, p13459-13481.

Walton, C.C., 1988, Nonlinear multichannel algorithms for estimating sea surface temperature with AVHRR satellite data. J. Applied Meteor., 27, p115-124.